Structures and Electrochemical Properties of $LiNi_{0.5-x}Co_{2x}Mn_{0.5-x}O_2$ as Cathode Materials for Lithium-ion Batteries

Hyun Chul Choi, Ho-Jin Kim,† Yeon Uk Jeong,†,* Soo-Hwan Jeong,‡ In Woo Cheong,§ and Uoo-Chang Jung#

Department of Chemistry, Chonnam National University, Gwangju, 500-757, Korea
†School of Materials Science and Engineering, Kyungpook National University, Daegu 702-701, Korea
**E-mail: jeong@knu.ac.kr*
‡Department of Chemical Engineering, Kyungpook National University, Daegu 702-701, Korea
§Department of Applied Chemistry, Kyungpook National University, Daegu 702-701, Korea
#Korea Institute of Industrial Technology, Busan 618-230, Korea
Received August 10, 2009, Accepted September 14, 2009

$LiNi_{0.5-x}Co_{2x}Mn_{0.5-x}O_2$ (x = 0, 0.1, 1/6, 1.2, 0.3) were synthesized by the solid-state reaction method. The crystal structure was analyzed by X-ray powder diffraction and Rietveld refinement. $LiNi_{0.5-x}Co_{2x}Mn_{0.5-x}O_2$ samples give single phases of hexagonal layered structures with a space group of R-3m for x = 0.1, 1/6, 0.2, and 0.3. The lattice constants of a and c-axis were decreased with the increase in Co contents in samples. The thickness of MO_2 slab was decreased and inter-slab distance was increased with the increase in Co contents in $LiNi_{0.5-x}Co_{2x}Mn_{0.5-x}O_2$. According to XPS analysis, the valence states of Mn, Co, and Ni in the sample are mainly +4, +3, and +3, respectively. The discharge capacity of 202 mAh/g at 0.1C-rate in the potential range of 4.7 - 3.0 V was obtained in $LiNi_{0.3}Co_{0.4}Mn_{0.3}O_2$ sample, and $LiNi_{0.4}Co_{0.2}Mn_{0.4}O_2$ gives excellent cycle performance in the same potential range.

Key Words: Secondary lithium batteries, Cathode materials, XRD, XPS, Electrochemical properties

Introduction

One of the advantages of secondary lithium batteries is high energy density as they have higher potentials than those of other rechargeable systems.[1] Layered host materials such as $LiCoO_2$ cathodes are widely used for commercial lithium-ion batteries as they exhibit reversible lithium intercalations.[2-3] There is increasing demand for alternative materials, and various materials with different structures were widely investigated.[4-8] $LiNi_{1-x}M_yO_2$ (M = Co, Mn, Al, Mg, *etc.*) materials were developed to achieve low cost, safety, or environmental concern.[9-11] The amounts of lithium intercalation of these materials mainly depend on the charge potential as well as the nickel contents in the compounds. Compared to $LiCoO_2$, these materials have low densities, electrical conductivities, and rate capabilities. $LiNi_{1-x}M_yO_2$ materials are generally synthesized by co-precipitation reaction followed by heating at high temperature.[11-12] In order to achieve improved energy densities of $LiNi_{0.5-x}Co_{2x}Mn_{0.5-x}O_2$ cathodes, it is important to enhance the structural stability of these layered compounds at higher charge potentials. In this research, the analysis of crystal structures and valence states of metal species for the samples prepared by solid-state reaction were systematically investigated, and the various electrochemical properties at different charge potentials are reported in this paper.

Experimental Section

$LiNi_{0.5-x}Co_{2x}Mn_{0.5-x}O_2$ (x = 0, 0.1, 1/6, 0.2, 0.3) samples were synthesized by solid-state reactions. Li_2CO_3, NiO, Co_3O_4, and MnO_2 as starting materials were milled with zirconia balls in ethyl alcohol for 24 hours. The ratio of Li : (Ni + Co + Mn) was adjusted to 1.05 : 1 to adjust lithium loss at high heating temperature. To remove ethyl alcohol, the mixtures of starting materials were dried in oven at 100 °C for 24 hours. Dried powders were heated at 1000 °C for 10 hours in air. X-ray powder diffraction and Rietveld refinement were carried out to analyze the crystal structure of the products.

The oxidation state of metal ions was investigated by X-ray photoelectron spectroscopy (XPS). The spectra were obtained with a VG multilab 2000 equipment (ThermoVG scientific) using non-monochromatized Mg K_α radiation (1253.6 eV). Core peaks were collected using a pass energy of 20 eV. No charge neutralization was used. The pressure in the analysis chamber was kept below 10^{-9} Pa. The binding energy scale was calibrated from the hydrocarbon contamination using the C 1s peak at 285.0 eV.

The electrochemical performances were evaluated by using coin cells (2016 type). Composite slurries were prepared by mixing of 95 wt% active material, 2 wt% acetylene black as a conductive additive and 3 wt% polyvinylidene fluoride (PVDF) as a binder and N-methyl pyrrolidone (NMP) as a solvent. Prepared slurries were coated onto aluminum foil of 30 μm thickness followed by drying in oven at 120 °C. Lithium metal was used as anode. For electrolytes, 1.15 M $LiPF_6$ was dissolved in the solution of ethylene carbonate (EC), dimethyl carbonate (DMC) and diethyl carbonate (DEC) with a ratio of 3:6:1. Coin cells were assembled in Ar-filled glove box. The charge/discharge test was performed between 4.7 V (or 4.3 V) and 3.0 V with different current densities (0.1C-rate, 0.2C-rate, 0.5C-rate, and 1C-rate), and 1C-rate was 140 mAh g^{-1}. Cyclability tests were carried out in the potential range of 4.7 - 3.0 V

with 0.2 C-rate charge and 1 C-rate discharge for 50 cycles.

Results and Discussion

Figure 1 shows X-ray powder diffraction patterns for $LiNi_{0.5-x}Co_{2x}Mn_{0.5-x}O_2$ (x = 0, 0.1, 1/6, 0.2, 0.3) samples. In the case of x = 0, impurity of Li_2MnO_3 was observed. However, single phase of hexagonal layer structure (R-3m) was successfully synthesized for samples of the other compositions. The results of Rietveld refinement using Fullprof program were shown in Figure 2. Table 1 summarizes the crystallographic data of $LiNi_{0.5-x}Co_{2x}Mn_{0.5-x}O_2$ (x = 0.1, 1/6, 0.2, 0.3) samples. The specific positions of oxygen (z_{oxygen}) were varied with Co contents. X-ray peak ratios of I_{003}/I_{104} were increased with the increase in x of $LiNi_{0.5-x}Co_{2x}Mn_{0.5-x}O_2$. Lattice constants of a and c-axis were decreased with the increase in Co contents in the samples, and these are shown in Figure 3. These results might be due to the less repulsion between metal ions in the lattice, because the radius of Co^{3+} ion has similar value of the average radius of Ni^{3+} and Mn^{4+} ions (r_{Co3+} = 0.545 Å, r_{Ni3+} = 0.56 Å, r_{Mn4+} = 0.53 Å). Bond lengths and angles between anion and cations are shown in Table 2 and Figure 4. While the bond length of Li-O increased with the increase in Co contents. M-O bond length were decreased with the increase in Co contents in the samples. In the case of the angles between ions, with the increase in Co contents in $LiNi_{0.5-x}Co_{2x}Mn_{0.5-x}O_2$, angles of O_1-Li-O_4 and O_1-M-O_2 were increased but angles of O_1-Li-O_2 and O_1-M-O_4 were decreased. These variations of bond length and angle change the thickness of MO_2 slab and

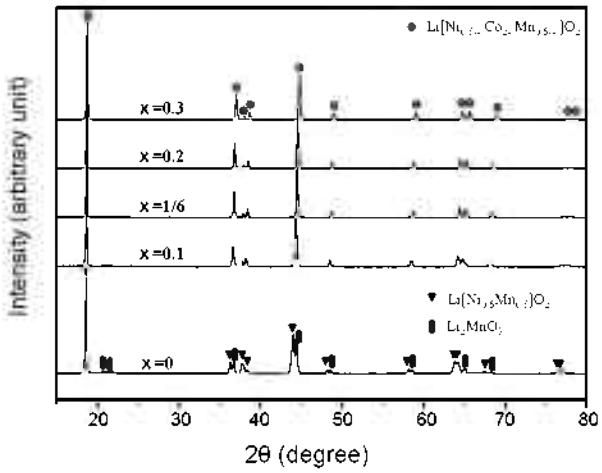

Figure 1. X-ray powder diffraction patterns of various $LiNi_{0.5-x}Co_{2x}Mn_{0.5-x}O_2$ phases.

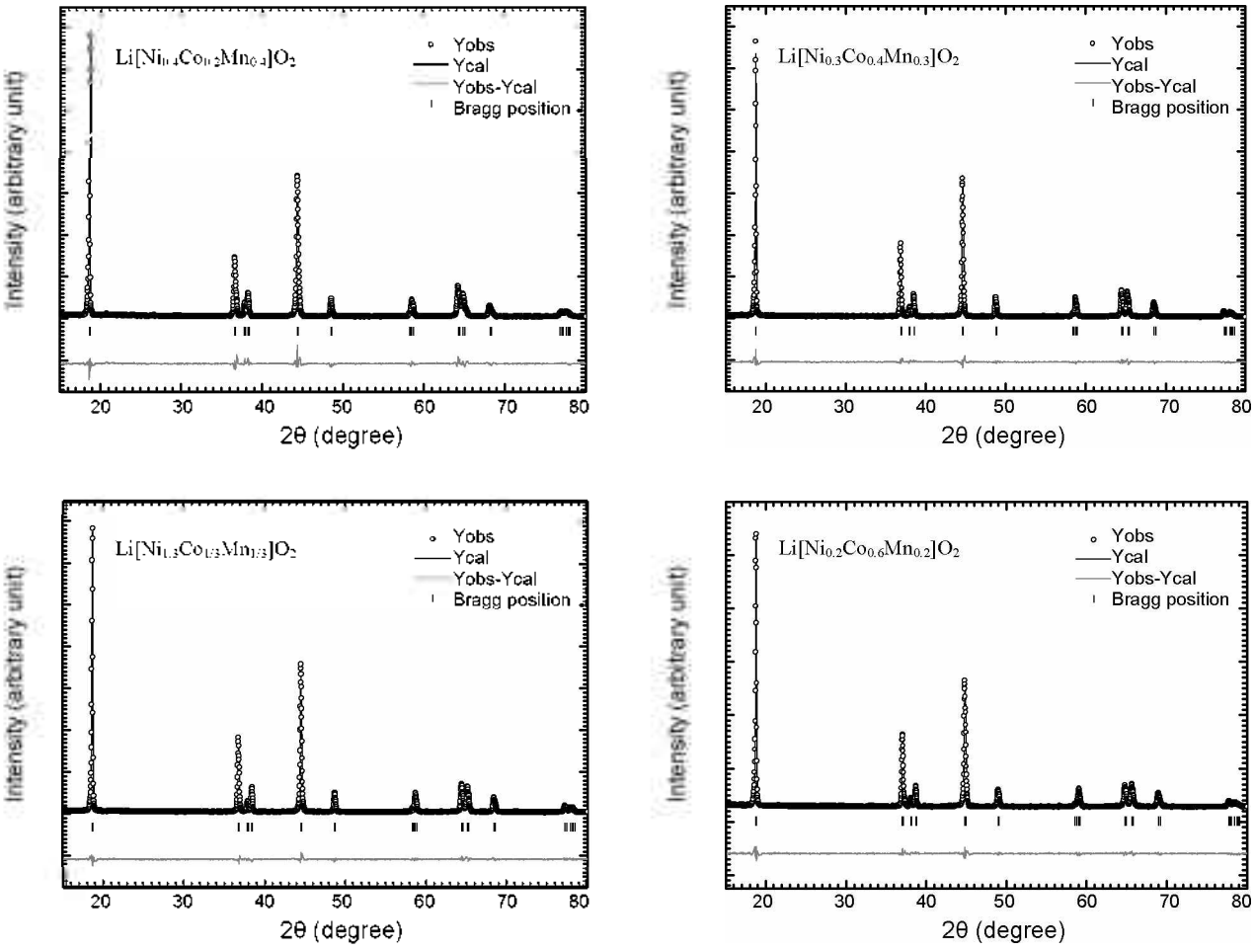

Figure 2. XRD patterns of $LiNi_{0.5-x}Co_{2x}Mn_{0.5-x}O_2$ phases by Rietveld refinement.

Table 1. Lattice constants, intensity ratios and specific positions of oxygen (z_{oxygen}) from Reitveld refinement for various $LiNi_{0.5-x}Co_{2x}Mn_{0.5-x}O_2$ samples.

$LiNi_{0.5-x}Co_{2x}Mn_{0.5-x}O_2$	a_{hex} (Å)	c_{hex} (Å)	c/a	I_{003}/I_{104}	z_{oxygen}	R_p	Chi^2
x = 0.1	2.8734	14.2561	4.961	1.07	0.24337	8.96	2.95
x = 1/6	2.8628	14.2378	4.973	1.24	0.24123	6.79	1.63
x = 0.2	2.8572	14.2225	4.978	1.28	0.24023	7.41	1.89
x = 0.3	2.8422	14.1736	4.987	1.38	0.23956	7.37	1.55

Table 2. The calculated cation-anion distance and angle from Rietveld refinement for various $LiNi_{0.5-x}Co_{2x}Mn_{0.5-x}O_2$ samples.

$LiNi_{0.5-x}Co_{2x}Mn_{0.5-x}O_2$	Distance (Å)		Angle (°)	
	Li-O	M-O	O_1-Li-O_2 / O_1-Li-O_4	O_1-M-O_2 / O_1-M-O_4
x = 0.1	2.0969	1.9869	86.49 / 93.51	92.62 / 87.38
x = 1/6	2.1098	1.9644	85.44 / 94.56	93.55 / 86.45
x = 0.2	2.1153	1.9534	84.96 / 95.04	94.00 / 86.00
x = 0.3	2.1156	1.9383	84.55 / 95.45	94.30 / 85.70

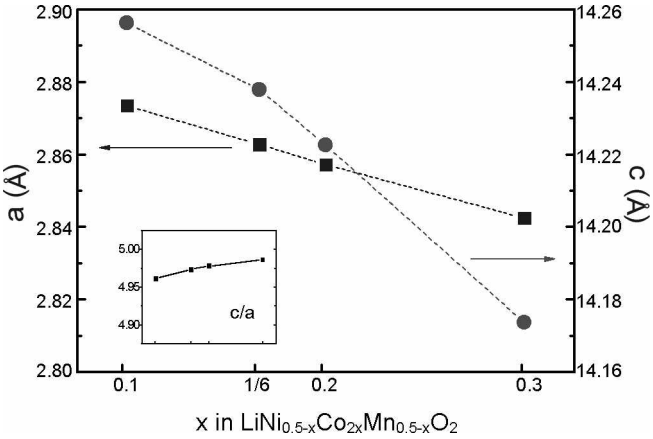

Figure 3. Lattice parameters of $LiNi_{0.5-x}Co_{2x}Mn_{0.5-x}O_2$ (x = 0.1, 1/6, 0.2, 0.3).

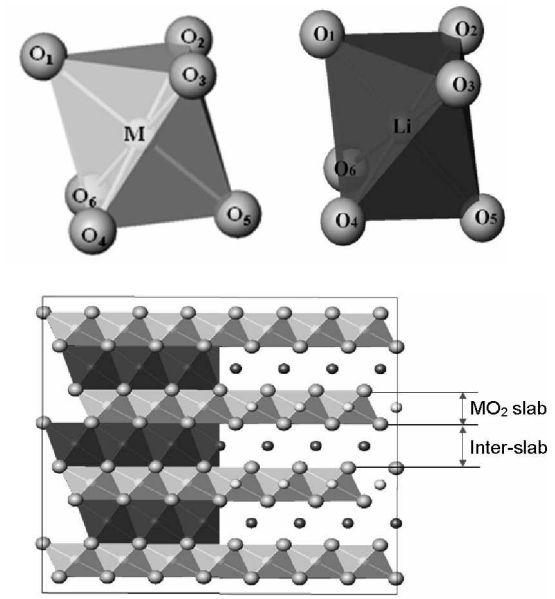

Figure 4. Structures of $LiNi_{0.5-x}Co_{2x}Mn_{0.5-x}O_2$.

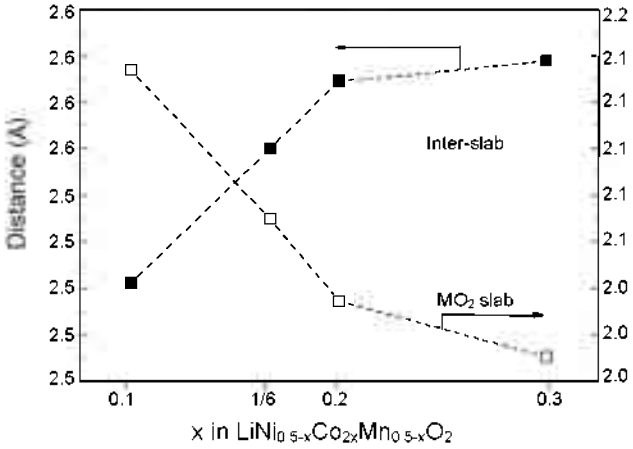

Figure 5. The calculated MO_2 slab thickness and inter-slab distance from Rietveld refinement.

inter-slab spacing. As shown in Figure 4 and Figure 5, increase in Co contents in $LiNi_{0.5-x}Co_{2x}Mn_{0.5-x}O_2$ resulted in the decrease in the thickness of MO_2 and the increase in the distance of inter-slab. Large inter-slab distance can be possibly related with easy intercalation of lithium ions in the lattice.

To elucidate the valence state of the transition metal species in the synthesized $LiNi_{0.5-x}Co_{2x}Mn_{0.5-x}O_2$ (x = 0.1, 1/6, 0.2, 0.3) samples, XPS analysis was carried out and the result is shown in Figure 6. The binding energies of an electron in Mn $2p_{3/2}$, Co $2p_{3/2}$, and Ni $2p_{3/2}$ are determined at 642.4, 780 and 855 eV,respectively. In Ni $2p_{3/2}$ spectra, a satellite peak is also detected at 861 eV due to the multiple splitting in the energy levels of the Ni-oxides. A noticeable shift of maximum of the photoemission line was not observed with increasing Co content. The observed values suggest that the valence states of Mn, Co, and Ni in the sample are mainly +4, +3, and +3, respectively, which are consistent with the previous results.[13-17]

Figure 7 shows S.E.M. images of various $LiNi_{0.5-x}Co_{2x}Mn_{0.5-x}O_2$ samples. Average particle sizes of the samples of x = 0, 0.1, 1/6, 0.2 and 0.3 in $LiNi_{0.5-x}Co_{2x}Mn_{0.5-x}O_2$ were 0.5, 0.7, 0.8, 1.0

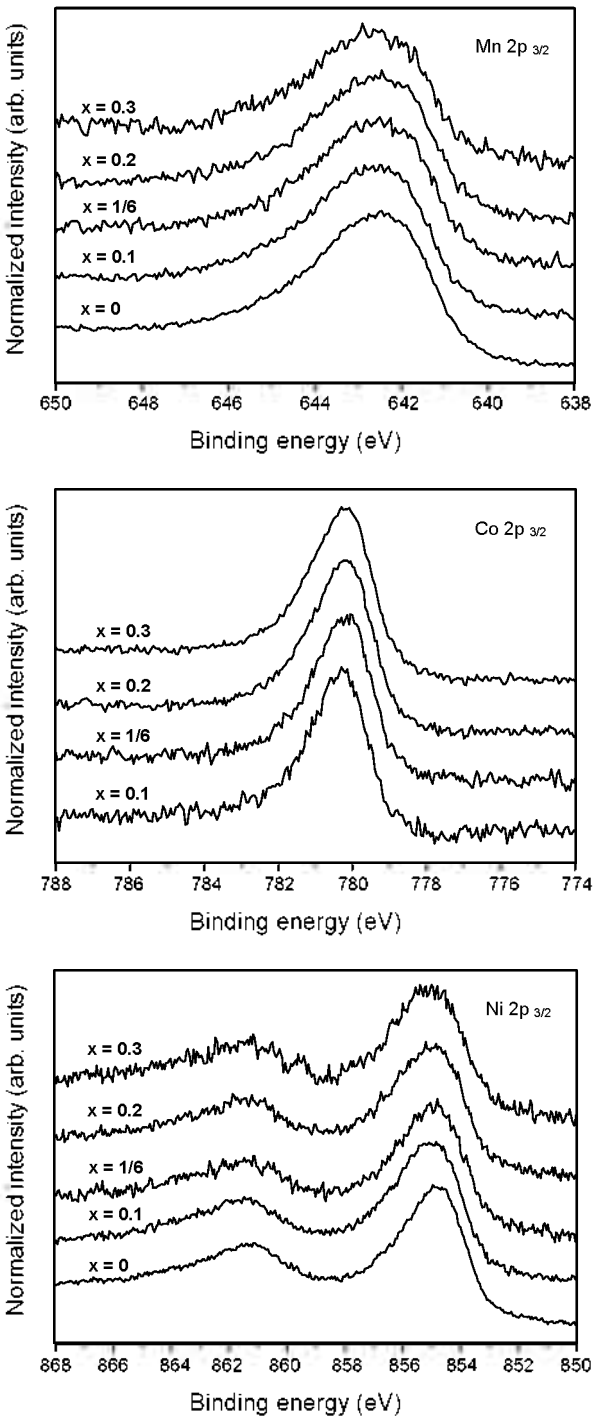

Figure 6. XPS spectra of Mn $2p_{3/2}$, Co $2p_{3/2}$ and Ni $2p_{3/2}$ for $LiNi_{0.5-x}Co_{2x}Mn_{0.5-x}O_2$ (x = 0, 0.1, 1/6, 0.2, 0.3) samples.

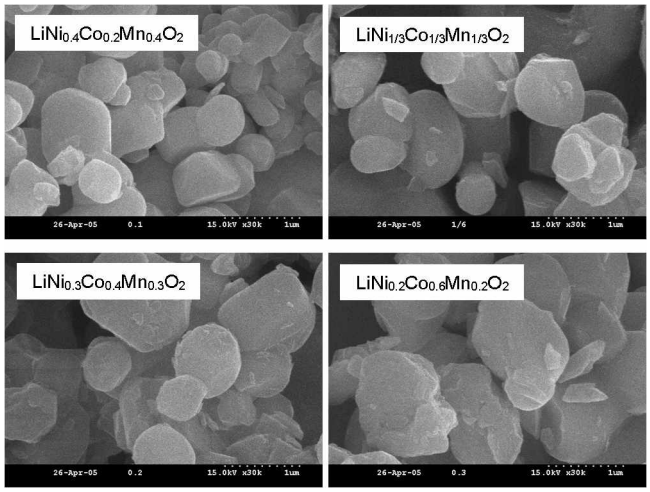

Figure 7. S.E.M. pictures of various $LiNi_{0.5-x}Co_{2x}Mn_{0.5-x}O_2$ powders.

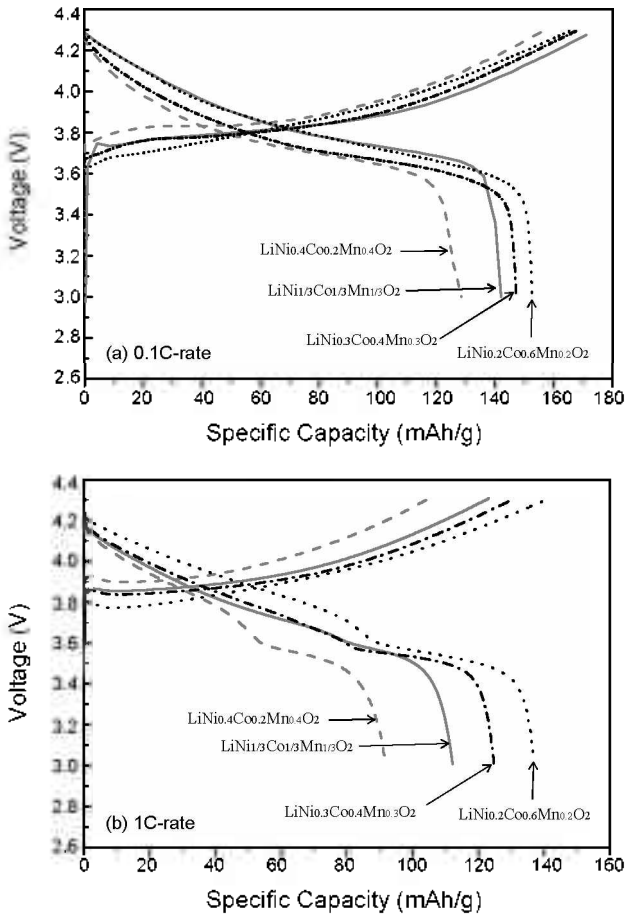

Figure 8. Charge-discharge profiles of $LiNi_{0.5-x}Co_{2x}Mn_{0.5-x}O_2$ (x = 0.1, 1/6, 0.2, 0.3) (voltage range: 4.3 - 3.0 V).

and 1.2 μm, respectively. The samples with higher Co contents tend to give the growth of particles. The charge and discharge profiles of potential ranges of 4.3 - 3.0 V are shown in Figure 8. The samples with higher Co contents exhibit larger discharge capacities with various C-rates. Figure 9 shows discharge profiles of potential range of 4.7 - 3.0 V for $LiNi_{0.4}Co_{0.2}Mn_{0.4}O_2$ and $LiNi_{0.3}Co_{0.4}Mn_{0.3}O_2$ samples. Discharge capacities were increased with the increase in charge potential in both samples. and $LiNi_{0.3}Co_{0.4}Mn_{0.3}O_2$ exhibit higher discharge capacities than the other. Results of cyclability test of $LiCoO_2$, $LiNi_{0.4}Co_{0.2}Mn_{0.4}O_2$ and $LiNi_{0.3}Co_{0.4}Mn_{0.3}O_2$ samples are shown in figure 10. While $LiCoO_2$ sample shows poor cycle performance in the potential range of 4.7 - 3.0 V, $LiNi_{0.4}Co_{0.2}Mn_{0.4}O_2$ and $LiNi_{0.3}Co_{0.4}Mn_{0.3}O_2$ samples exhibit enhanced cycle lives. Though smaller discharge capacity was observed in $LiNi_{0.4}Co_{0.2}$

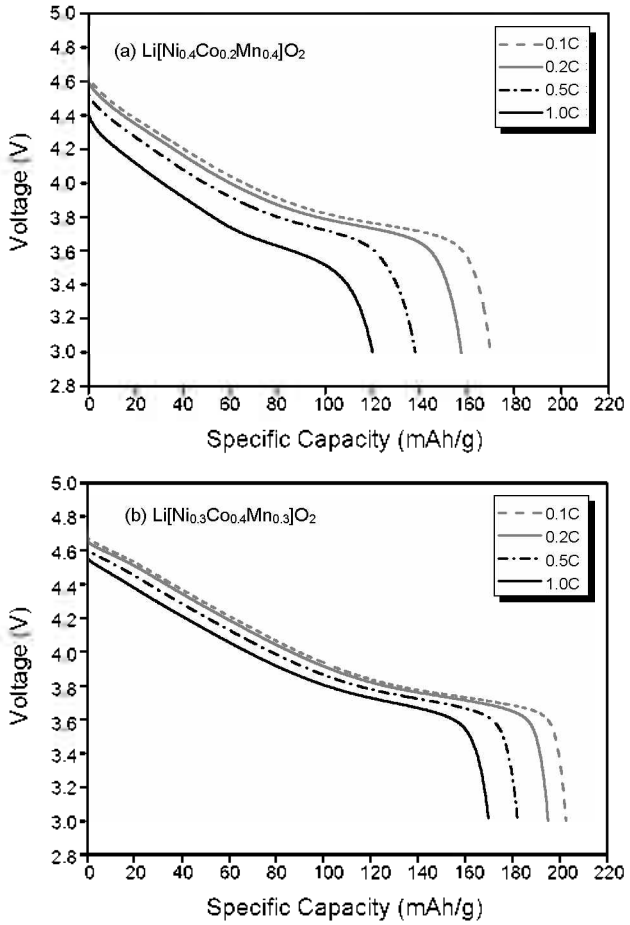

Figure 9. Discharge profiles of $LiNi_{0.5-x}Co_{2x}Mn_{0.5-x}O_2$ (x = 0.1, 0.2) (voltage range: 4.7 - 3.0 V).

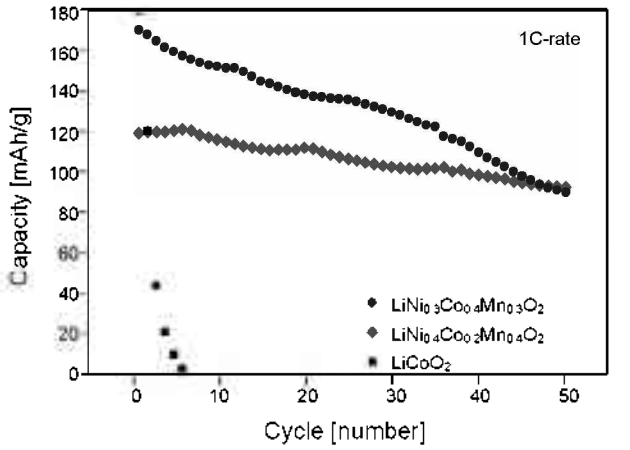

Figure 10. Cycling performances of $LiCoO_2$, $LiNi_{0.4}Co_{0.2}Mn_{0.4}O_2$, and $LiNi_{0.3}Co_{0.4}Mn_{0.3}O_2$ with 0.2 C-rate charge and 1.0 C-rate discharge (voltage range: 4.7 - 3.0 V).

$Mn_{0.4}O_2$ samples, it had better capacity retention than $LiNi_{0.3}Co_{0.4}Mn_{0.3}O_2$. Compared to $Co^{3+/4+}$ d band, $Ni^{3+/4+}$ d band has less overlap with O^{2-} 2p band, oxygen loss in the lattice can be reduced during the delithiation process.[18] Improved cycle performance might be due to the increased lattice stability on high charge potential.

Conclusion

$LiNi_{0.5-x}Co_{2x}Mn_{0.5-x}O_2$ (x = 0.1, 1/6, 0.2, 0.3) samples were synthesized by solid-state reactions, and single phase of hexagonal layered structures were obtained. The results of Rietveld refinement give lattice constants, bond lengths and angles. Lattice constants of a and c-axis were decreased with the increase in Co contents due to less ionic repulsion in the lattice. With the increase of Co contents in the samples, the bond lengths of Li-O, the angles of O_1-Li-O_4 and O_1-M-O_2 were increased, however the bond lengths of M-O, the angles of O_1-Li-O_2 and O_1-M-O_4 were decreased. As the result from these, MO_2 slab thickness was decreased and inter-slab distance was increased with the Co contents in the samples. The XPS analysis indicates that the valence states of Mn, Co, and Ni in the samples are mainly tetravalent, trivalent, and trivalent, respectively.

The samples with higher Co contents exhibit larger discharge capacities with various C-rates in the potential range of 4.3 - 3.0 V. $LiNi_{0.3}Co_{0.4}Mn_{0.3}O_2$ sample shows discharge capacity of 202 mAh/g at 0.1C-rate, and $LiNi_{0.4}Co_{0.2}Mn_{0.4}O_2$ gives excellent cycle performance in the potential range of 4.7 - 3.0 V. Compared to $LiCoO_2$, enhanced cycle performances of these materials are due to the increased lattice stability on high charge potential.

References

1. Armand, M. *Solid State Ionics* **1994**, *69*, 309.
2. Mitzushima, K.; Jones, P. C.; Wiseman, P. J.; Goodenough, J. B. *Mater. Res. Bull.* **1980**, *15*, 783.
3. Yoshio, M; Tanaka, H.; Tomonaga, K.; Noguchi, H. *J. Power Sources* **1992**, *40*, 347.
4. Padhi, K.; Nanjundaswamy, K. S.; Goodenough, J. B. *J. Electrochem. Soc.* **1997**, *144*, 1188.
5. Thackeray, M. M.; Shao-Horn, Y.; Kahaian, A. J.; Kepler, K. D.; Skinner, E.; Vaughey, J. T.; Hackney, S. A. *Electrochem. Solid-State Lett.* **1998**, *1*, 7.
6. Wen, S. J.; Richardson, T. J.; Ma, L.; Striebel, K. A.; Ross, P. N.; Cairns, E. J. *J. Electrochem. Soc.* **1996**, *143*, L136.
7. Doeff, M. M.; Peng, M. Y.; Ma, Y.; De Jonghe, L. C. *J. Electrochem. Soc.* **1994**, *141*, L145.
8. Paulsen, J. M.; Thomas, C. L.; Dahn, J. R. *J. Electrochem. Soc.* **2000**, *147*, 2862.
9. Saadoune, I.; Delmas, C. *J. Solid State Chem.* **1998**, *136*, 8.
10. Wang, Y.; Jiang, J.; Dahn, J. R. *Electrochem. Commun.* **2007**, *9*, 2534.
11. Yabuuchi, N.; Ohzuku, T. *J. Power Sources* **2003**, *119-121*, 171.
12. Bommel, A. V.; Dahn, J. R. *Chem. Mater.* **2009**, *21*, 1500.
13. Shaju, K. M.; Subba Rao, G. V.; Chowdari, B. V. R. *Electrochim. Acta* **2002**, *48*, 145.
14. Shaju, K. M.; Subba Rao, G. V.; Chowdari, B. V. R. *Electrochim. Acta* **2003**, *48*, 1505.
15. Li, D.; Kata, Y.; Kobayakawa, K.; Noguchi, H.; Sata, Y. *J. Power Sources* **2006**, *160*, 1342.
16. Kosova, N. N.; Devyatkina, R. T.; Kaichev, V. V. *J. Power Sources* **2007**, *174*, 965.
17. Guo, R.; Shi, P.; Cheng, X.; Du, C. *J. Alloys Compd.* **2009**, *473*, 53.
18. Chebiam, R. V.; Prado, F.; Manthiram, A. *Chem. Mater.* **2001**, *13*, 2951.